

Copper Indium Sulfide Quantum Dots as Nanomanometers: Influence of Size and Composition

Leyre Aldaz-Caballero, Ulises R. Rodríguez-Mendoza, Víctor Lavín, Patrizia Canton, Antonio Benayas,* and Riccardo Marin*


Mechanical forces control the function of organisms and mediate the interaction between biological systems and their environments. Knowledge of these forces will increase the understanding of biological processes and can support the development of novel diagnostic and therapeutic procedures. Although techniques like atomic force microscopy and droplet insertion method allow measuring forces over a broad range of values, they are invasive and lack versatility. A promising way to overcome these hurdles is luminescent nanomanometry. Quantum dots (QDs) specifically have optical properties that depend on their size because of the quantum confinement, which makes them responsive to applied forces. Yet, a fine understanding of how fundamental parameters affect the response to applied stress is required before a QD family can be credibly proposed as luminescent nanomanometers. Here, a thorough study is conducted on how size and stoichiometry affect the nanomanometry performance of CuInS_2 QDs. The studied QDs feature pressure-dependent photoluminescence in the red/near-infrared range, which can enable the measurement of mechanical forces in the range of physiological relevance in a remote and minimally invasive way. It is shown that tuning size and stoichiometry can simultaneously enhance the CuInS_2 QDs' brightness and response to applied pressure, thus providing guidelines for better luminescent nanomanometers.

1. Introduction

Living organisms are constantly interacting with the surrounding environment, receiving and transmitting signals. Among these signals, mechanical forces are ubiquitous, spanning different orders of magnitude.^[1] In the human body, they range from the Newton scale at the organ level to the nanoNewton (nN) forces that drive tumor progression, all the way down to the picoNewton (pN) forces involved in integrin-mediated cell adhesion.^[2] Full knowledge of these forces would allow to reach a deeper understanding of biological processes and develop more effective diagnostic and therapeutic tools. In this context, the measurement of forces at the (sub)cellular level and, ideally, in physiological conditions represents a great challenge. Some techniques for measuring forces in biological systems, like atomic force or traction force microscopies, require the removal of the cells from

L. Aldaz-Caballero, A. Benayas, R. Marin
Nanomaterials for Bioimaging Group (nanoBIG)
Facultad de Ciencias
Universidad Autónoma de Madrid
C/ Francisco Tomás y Valiente 7, Madrid 28049, Spain
E-mail: antonio.benayas@uam.es; riccardo.marin@uam.es
U. R. Rodríguez-Mendoza, V. Lavín
Departamento de Física
MALTA-Consolider Team
IMN and IUdEA
Universidad de La Laguna
Apdo. de Correos 456, San Cristóbal de La Laguna, Santa Cruz de Tenerife
E-38200, Spain

P. Canton
Department of Molecular Sciences and Nanosystems
Ca' Foscari University of Venice
Via Torino 155/b, Venezia-Mestre I-30170, Italy
A. Benayas, R. Marin
Instituto Nicolás Cabrera
Universidad Autónoma de Madrid
Madrid 28049, Spain
A. Benayas
Nanomaterials for Bioimaging Group (nanoBIG)
Instituto Ramón y Cajal de Investigación Sanitaria (IRICYS)
Hospital Ramón y Cajal
Ctra. De Colmenar Viejo km 9.100, Madrid 28034, Spain
R. Marin
Institute for Advanced Research in Chemical Sciences (IAdChem)
Universidad Autónoma de Madrid
Madrid 28049, Spain

 The ORCID identification number(s) for the author(s) of this article can be found under <https://doi.org/10.1002/adsr.202300078>

© 2023 The Authors. Advanced Sensor Research published by Wiley-VCH GmbH. This is an open access article under the terms of the Creative Commons Attribution License, which permits use, distribution and reproduction in any medium, provided the original work is properly cited.

DOI: 10.1002/adsr.202300078

their natural environment and introduction in an artificially controlled medium.^[3] Other techniques like optical tweezers have been used for both in vitro and in vivo measurements,^[4] but proper calibration is challenging and time-consuming. While these techniques were key for moving the first steps toward understanding forces at the subcellular level, they hardly have the versatility to garner information about biomechanical forces in physiological conditions.

In this context, luminescent nanoproboscopes are promising candidates because they rely on light emission changes for sensing and have small size. This combination allows measurements to be performed remotely and in a minimally invasive way.^[5] The development of suitable luminescent nanoproboscopes requires fine optimization of several parameters to increase the sensitivity toward forces of the magnitude of interest and maintain high brightness, (i.e., the product between light absorption and emission efficiency). These are two features that, combined, ensure reliable readout.^[6] When it comes to pressure sensing (i.e., luminescence manometry), great strides have been made using lanthanide and transition metal-doped luminescent materials. Dionne and co-workers have been at the forefront in this field, being among the first to report upconverting nanoparticles as pressure sensors,^[2a] which opened the door to several works on luminescence manometry and combined manometry-thermometry.^[7] Recently the use of transition metal-doped materials has also witnessed a surge, with the report of the highest relative sensitivity so far (120% GPa⁻¹).^[8] On the other hand, quantum dots (QDs) have emerged as prime nanosensors.^[7a,9] This is because quantum confinement effects at the nanoscale allow tuning the optical properties of QDs by controlling their size,^[10] hence making them sensitive to applied mechanical forces.^[11] Indeed, when a QD is exposed to external mechanical pressure, i.e., the force-to-surface ratio, its volume is effectively reduced, thus resulting in a blueshift of the emission band. Moreover, the pressure-induced changes in interatomic distances yield variations in the overlap between orbitals, ultimately affecting the electronic band structure. These combined effects are the main ones responsible for the pressure sensitivity of the emission of QDs, thus making them suitable probes in luminescence nanomanometry. Importantly, reports in the literature show responses from ambient pressure up to several gigapascal (GPa): values that seem excessively large eyeing biological processes. However, given the small size of QDs (generally below 10 nm in diameter) and the corresponding surface area, these pressures translate to forces experienced by a single QD in the nN-to- μ N range (Figure 1): the characteristic magnitude of several biomechanical forces of interest.

Among QDs, those made of copper indium sulfide (CIS)^[12] are uniquely attractive for the development of luminescence nanomanometry approaches targeting biological applications. One advantage offered by this material is its lower toxicity compared to Cd- and Pb-based QDs.^[13] More essentially for their sensing role, the emission of CIS QDs can be tuned by tweaking different parameters like size, chemical composition, crystal structure, and core/shell architecture. Concerning pressure sensing, Wang, J. et al. showed that CIS QDs have pressure sensitivity in the GPa range.^[5b] They also proved that the growth of a ZnS shell enhanced the photoluminescence while making them less susceptible to plastic deformations.^[5b] Yet, the role that size and

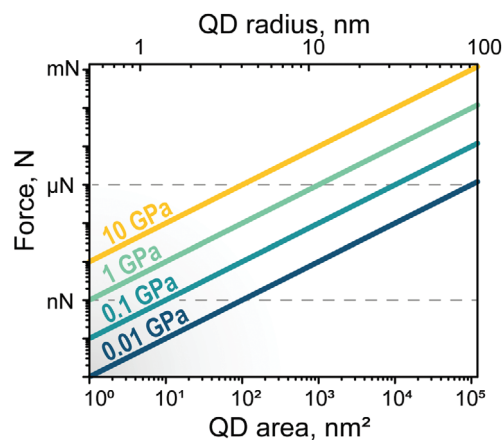


Figure 1. Pressure to force conversion for QDs. A spherical QD of variable radius is considered. Each solid line corresponds to a different pressure value.

composition play in modulating the response of CIS QDs to applied pressure is still unknown.

In this work, we provide an answer to this question by investigating the behavior of different CIS QDs synthesized via a microwave (MW)-assisted method. This method affords control of the reaction time and relative amount of Cu⁺ and In³⁺ precursors, thus enabling fine-tuning of the size and stoichiometry (i.e., Cu/In ratio) of the QDs. The response of the QDs to applied pressure was investigated in a diamond anvil cell (DAC), consistently observing a blueshift of the photoluminescence peak. The trends in the response to applied pressure as a function of size and stoichiometry are interpreted and quantified, highlighting how the intentional introduction of Cu⁺ vacancies in CIS QDs affords a more reliable pressure readout alongside more intense emission. As a result, a new family of upgraded optical nanomanometers was produced.

2. Results and Discussion

2.1. Preparation and Characterization of CuInS₂ Quantum Dots

The two series of CIS QDs were prepared according to the MW-assisted procedure outlined in the Experimental Section and are summarized in Table 1. The size of the QDs was tuned by varying the reaction time from 2.5 to 10 min, with steps of 2.5 min. Control over the stoichiometry was instead achieved by changing the relative ratio of metal precursors introduced in the reaction mixture. The composition of the QDs was determined via total reflection X-ray fluorescence (TXRF), observing Cu/In values close to 1.3 for the samples composing the size series (CIS-2.5, 5, 7.5, 10) and a gradually decreasing value for the stoichiometry series from CIS*1.0 to CIS*0.6 (Table 2). The deviation from the theoretical Cu/In value in the size series can be a result of a slightly more efficient incorporation of Cu⁺ ions than In³⁺ ions or of the existence of a copper-rich surface, which is to be expected since the 1-dodecanethiol molecules attached to the QD surface have a higher affinity for copper.^[12a] X-ray powder diffraction (XRPD) measurements confirmed that all the prepared QDs have a chalcopyrite (*I*-42d) crystal structure (Figure S1, Supporting

Table 1. Summary of the samples synthesized in this work changing the reaction time (size series) and the precursor ratio (stoichiometry series). All the samples were prepared at 240 °C. Samples CIS-7.5 and CIS*1.0 are the same sample.

	Sample ID	Reaction time, min	Cu/In ratio (nominal)
Size series	CIS-2.5	2.5	1.0
	CIS-5	5	1.0
	CIS-7.5	7.5	1.0
	CIS-10	10	1.0
Stoichiometry series	CIS*1.0	7.5	1.0
	CIS*0.8	7.5	0.8
	CIS*0.7	7.5	0.7
	CIS*0.6	7.5	0.6

Table 2. Size of the CIS QDs investigated in this study obtained from the Scherrer equation, effective mass approximation (EMA),^[10c,12b,14,17] and position of the photoluminescence peak (Booth's approach),^[16] alongside their composition as determined from TXRF measurements. CIS-7.5 and CIS*1.0 are the same samples (in bold).

Sample	Scherrer (nm)	EMA (nm)	Photoluminescence (nm)	TXRF	
				Cu/In	S/In
CIS-2.5	2.3 ± 0.1	2.8 ± 0.4	3.9 ± 0.1	1.25	2.26
CIS-5	2.6 ± 0.1	2.9 ± 0.2	4.5 ± 0.1	1.31	2.37
CIS-7.5 / CIS*1.0	2.7 ± 0.1	2.9 ± 0.2	4.7 ± 0.1	1.35	2.3
CIS-10	2.9 ± 0.1	3.1 ± 0.1	5.4 ± 0.1	1.30	2.22
CIS*0.8	–	–	–	1.13	2.14
CIS*0.7	–	–	–	0.83	2.75
CIS*0.6	–	–	–	0.77	2.49

Information) and transmission electron microscopy (TEM) observations showed QDs with a morphology comparable with the expected tetrahedral habitus and sizes below 5 nm (from 2.5 to 4.3 nm; Figures S2–S8, Supporting Information). This piece of information underscored that the QDs were all in quantum confinement regime, since the exciton Bohr radius (a_B) of chalcopyrite CuInS₂ is 4.1 nm and all the QDs of this study have a radius $r < a_B$.^[14] The poor contrast provided by CIS QDs makes it challenging to accurately measure their size from TEM micrographs, yet a general trend of increasing size can be observed with increasing reaction time. To quantify this change in the size series, indirect approaches were also used. The Scherrer equation was applied to the (112) reflection centered at $\approx 28^\circ$, thus extracting from the X-ray diffraction patterns an average crystallite (i.e., the coherent crystal domain) size ranging from 2.3 to 2.9 nm (Table 2).

Information about the QD size can also be obtained from the analysis of extinction and photoluminescence spectra (Figure 2; Figure S9, Supporting Information). This is because the increase (decrease) in the size of a QD is accompanied by a red (blue) shift of the absorption and photoluminescence spectra. Upon fitting the linear part of the Tauc plot derived from the extinction spectra (inset in Figure 2a), the energy gap value (E_g) was obtained from the intersection of the fitting line with the x-axis. According

Table 3. Photoluminescence quantum yield (PLQY) of the reference (Rhodamine 110) and the samples of the stoichiometry series.

Sample	PLQY (%)
Rhodamine 110	85 (tabulated) ^[19]
CIS*1.0	4.1
CIS*0.8	4.5
CIS*0.7	7.0
CIS*0.6	6.9

to the effective mass approximation,^[15] the size of a QD can be inferred indirectly from the magnitude of its E_g if the properties of the bulk material are known (see details in the Supporting Information). Through this approach, values between 2.8 and 3.1 nm were calculated for the size series (Table 2).^[14] Lastly, the sizes of CIS QDs were also estimated from their photoluminescence peak position according to the empirical equation proposed by Booth et al. (details in the Supporting Information),^[16] obtaining values between 3.9 and 5.4 nm (Table 2). The values of size extracted from the three described approaches (Scherrer equation, effective mass approximation, and photoluminescence peak position) show a clear trend of increasing size with increasing reaction time, also agreeing well with the size estimated from TEM observations. Discrepancies between the three indirect approaches used for determining the size were expected given the different assumptions and definition of “size” in each case (e.g., the morphology factor in the Scherrer equation cannot be determined accurately, while Booth's approach considers as size approximately the height of a tetrahedron.)

In the case of the stoichiometry series, the three proposed indirect approaches are not applicable. The introduction of Cu⁺ vacancies in the lattice brings about lattice distortions and atomic displacement disorder that contribute to the broadening of the X-ray pattern reflections. The Scherrer approach cannot discriminate the broadening originating from size reduction and increased disorder. As such, the crystallite size cannot be reliably determined using this approach. The optical methods also fall short when the stoichiometry is changed because the introduction of Cu⁺ vacancies – here confirmed via TXRF measurements – modifies the composition of the electronic bands, leading to a blue shift of the absorption and photoluminescence spectra. Therefore, the observed optical changes cannot be unequivocally correlated with size changes.

Most importantly, the deliberate introduction of a sub-stoichiometric amount of Cu⁺ ions in the reaction environment translates to an increase in the photoluminescence quantum yield (PLQY) of the QDs (Table 3; Figure S10, Supporting Information). This effect is well-known, and it directly stems from the emission mechanism in CIS QDs, wherein the electron-hole radiative recombination occurs involving conduction band and localized Cu⁺ vacancy-related intraband states.^[18] Thus, a deliberate increase in the latter type of states via the introduction of sub-stoichiometric amounts of Cu⁺ supports a more efficient photoluminescence. For the studied samples, CIS*0.7 shows the highest PLQY value on par with sample CIS*0.6. This aspect indicates that a balance is reached with these compositions between the beneficial introduction of Cu⁺ vacancy-related

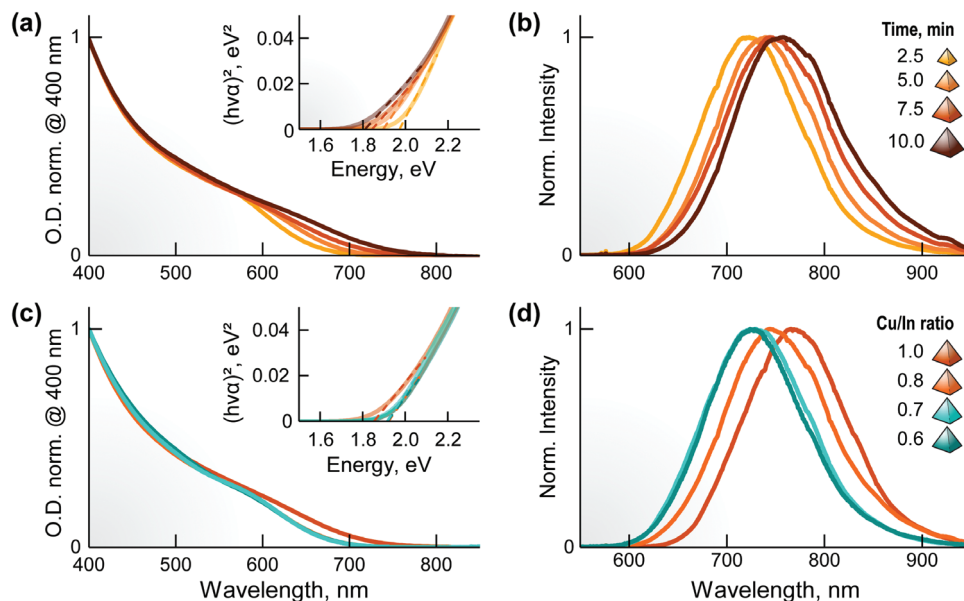


Figure 2. Optical characterization of the two series (size and stoichiometry) of CIS QDs. Extinction a,c) and emission b,d) spectra for the QDs of the size (top) and stoichiometry (bottom) series. Insets in (a) and (c) are the corresponding Tauc plots. Dashed lines therein are linear fits to extract the bandgap values. Emission spectra were recorded under 488 nm excitation. All measurements were performed in toluene. O.D. is optical density.

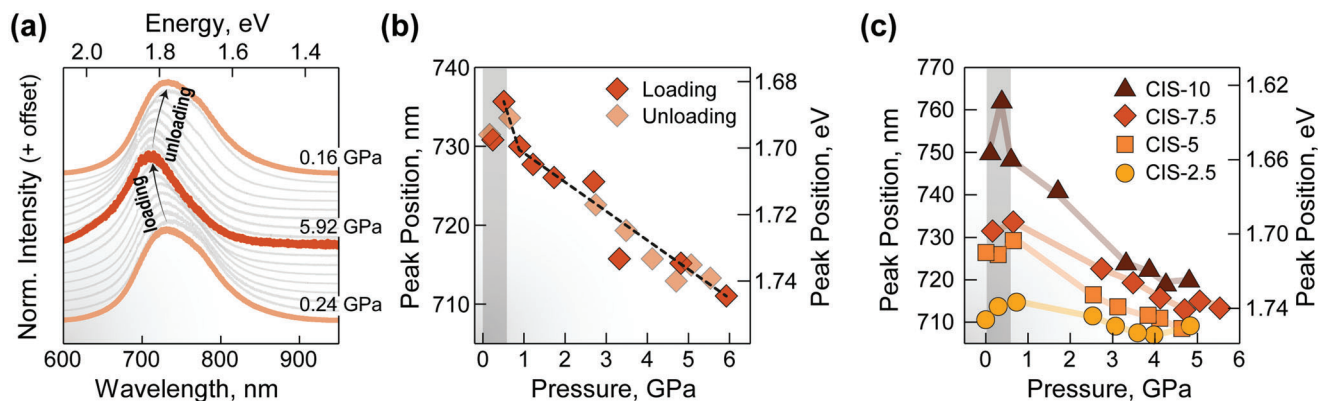


Figure 3. Calibration of the size series. a) Emission spectra under 532-nm excitation during compression and decompression cycles in a DAC. b) Peak position in wavelength and energy versus applied pressure for the CIS-7.5 (i.e., CIS-1.0) sample obtained from the compression and decompression cycles. The black dashed line is the double-linear fit to the experimental data. c) Comparison of the peak position change as a function of applied pressure during the compression cycle for all the samples of the size series. The grey rectangles in (b) and (c) indicate the pressure range where the initial redshift is observed.

energy levels and structural integrity of the QDs, respectively supporting stronger photoluminescence and negatively affecting the optical performance. Importantly, samples with lower Cu^+ content were also prepared but showed poorer colloidal stability and large size distribution. As such, they were not investigated further. The higher PLQY is pivotal in the context of luminescence sensing and hence in luminescence nanomanometry too, since the product of PLQY and molar absorption coefficient (i.e., brightness) directly translates to a higher signal-to-noise ratio when all other measurement conditions are fixed. As a result, a higher precision of the measurements is observed.^[20]

In summary, the results of the physicochemical and spectroscopic characterization of the two series of CIS QDs confirm that all the samples were obtained in the same crystalline structure

changing independently size or stoichiometry, thus laying the foundations for the investigation of the effect of these two parameters on the response to applied pressure.

2.2. Effect of Size on the Sensitivity to Applied Pressure

Reports in the literature point to a size dependence of mechanical - alongside optical - properties of QDs.^[21] Therefore, we set to study the effect that size has on the response to the pressure of CIS QDs. As a representative example of the size series, the change in the photoluminescence spectrum of the sample CIS-7.5 is proposed in Figure 3a (all the samples belonging to this series are presented in Figures S11–S14, Supporting

Information). During the compression cycle (0.24→5.92 GPa), the photoluminescence peak experiences a blueshift of ≈ 20 nm (60 meV) corresponding to 3.5 nm GPa^{-1} ($10.6 \text{ meV GPa}^{-1}$), followed by a regain of the initial peak position during the decompression cycle (5.92→0.16 GPa) (Figure 3b). This behavior could be explained by a size reduction induced by the application of pressure, hence leading to a bandgap widening according to the quantum confinement effect. Using Booth's empirical expression,^[16] the shift in the photoluminescence peak position would correspond to a change in volume of 40% following the application of approximately 6 GPa of pressure.^[22] The resulting bulk Young modulus would therefore be roughly 15 GPa: much smaller than the bulk value of $\approx 65 \text{ GPa}$.^[23] This indicates a contribution to the observed spectral shift coming from other factors, likely electron band restructuring. The lack of hysteresis (observed also in other samples of this series, see Supporting Information) underscores that the CIS QDs behave elastically in the explored pressure range: a fundamental prerequisite for their use as nanomanometers. Indeed, Li, Y. et al. previously showed irreversible chalcopyrite-to-cubic crystal phase transition in CIS QDs accompanied by photoluminescence quenching only above 9 GPa.^[24] The blueshift observed in this study is preceded by a redshift at pressures below 1 GPa. While the magnitude of this initial redshift is relatively small (≈ 5 nm) for CIS-7.5, and could be considered within the experimental variability, it was observed during both the compression and decompression cycles. Moreover, it also appeared in the other samples of the series (Figure 3c), suggesting that this behavior is intrinsic to the CIS QDs reported in this study when subjected to hydrostatic pressure. A tentative explanation of this trend is provided further below upon comparison with the stoichiometry series. Aside from this initial redshift, all the samples show a doubly linear trend, with a first steeper blueshift followed by a second more gradual change in peak position. This behavior was already observed in the literature in core-only CIS QDs,^[5b] but no final explanation was provided. We argue that it is probably related to a discontinuity in the mechanical behavior of CuInS_2 following pressure-induced densification. The change in the peak position for the different ranges is given in Table S1 (Supporting Information).

When the reaction time, and hence the QD size, is increased, the overall change in energy of the peak position becomes more pronounced. This shift was calculated neglecting the initial redshift, obtaining overall changes in the peak position of 1.4, 2.7, 3.4, and 5.9% for the samples CIS-2.5, 5, 7.5, and 10 respectively. The origin of this trend is likely to be searched in the increase in bulk modulus generally observed when the size of the QDs decreases, making smaller nanomaterials less sensitive to compression.^[25] The bandgap pressure coefficient (α) calculated for the studied CIS QDs (in the 3 to 21 meV GPa^{-1} range) is smaller in absolute value than the ones found in the literature for most binary QDs under hydrostatic compression, like those of CdSe (27 to 82 meV GPa^{-1}), PbSe (-41 to -81 meV GPa^{-1}), or InAs (91 meV GPa^{-1}) (see also Table S3, Supporting Information). The other study on luminescent CIS QDs subjected to mechanical compression found values up to $\approx 60 \text{ meV GPa}^{-1}$.^[5b] This discrepancy can tentatively be imputed to differences in the synthetic method, which only entails 1-dodecanethiol simultaneously as solvent, ligand, and sulfur source and the use of a classical heating synthesis method (as opposed to our MW-assisted

approach). Overall, this might lead to differences in the QD surface chemistry, composition, and microstructure.^[26]

Returning to our samples, although CIS-10 shows a more marked change, it is less suited for sensing purposes, because it reaches a plateau around 3.5–4 GPa and it does not completely recover the initial peak position when the pressure is released. Sample CIS-7.5 shows, therefore, the best tradeoff in terms of lack of hysteresis (see also Figure S15, Supporting Information), maximized change in peak position, and operational working range. For these reasons, it was selected as the starting point for studying the effect of varying stoichiometry.

2.3. Effect of Stoichiometry on the Sensitivity to Applied Pressure

As demonstrated above, the deliberate introduction of Cu^+ vacancies allows for increasing the PLQY of CIS QDs. However, the lattice distortion and disorder caused by these vacancies are also expected to modulate the change in pressure sensitivity of the QDs. To explore this possibility, a series of measurements like the ones described above were performed on the stoichiometry series (Figure 4). Taking sample CIS*0.8 as representative of the series, a blueshift of the emission peak could be observed upon application of pressure, without noticeable hysteresis during the decompression cycle (Figure 4a,b). This behavior is observed in all the samples of the series with the overall relative change in the position of the emission maxima of 3.4, 4.0, 4.6, and 2.8% for the samples CIS*1.0, 0.8, 0.7, and 0.6, respectively (Figure 4c; Figures S16–S18, Supporting Information). Notably, no initial uptick in the peak position, i.e., redshift, is observed in the samples with the sub-stoichiometric nominal copper amount. Yet, a more marked double-linear trend appeared, with a reduction in slope occurring invariably around 1 GPa. The change in the peak position for the different ranges is given in Table S2 (Supporting Information). Given that all the QDs investigated in this study have the same surface chemistry, the different behavior during compression cannot be attributed to surface effects. We argue that this is instead to be attributed to the change in the composition of the crystalline matrix.

In studies with lanthanide-doped nanoparticles, it was shown that the introduction of strain at the core-shell interface induced a higher sensitivity to applied pressure.^[27] Introduction of Cu^+ vacancies in the CIS lattice is bound to introduce strain and disorder, likely making them more susceptible to pressure-induced structural changes, while not having a sizeable impact on the elastic behavior.

2.4. Comparison of the Pressure Sensing Performance

Lastly, we quantified the performance of the investigated CIS QDs as luminescent nanomanometers, calculating their relative pressure sensitivity (S_r) and pressure resolution (δP) according to the guidelines outlined for luminescence nanothermometry (Figure 5). The used equations are provided in the Experimental Section. Only the *stoichiometry series* was analyzed as it also contains the best sample of the *size series* (CIS-7.5 = CIS*1.0).

As discussed above, all the samples show a doubly linear trend (see dashed lines in Figures S19–S22, Supporting Information),

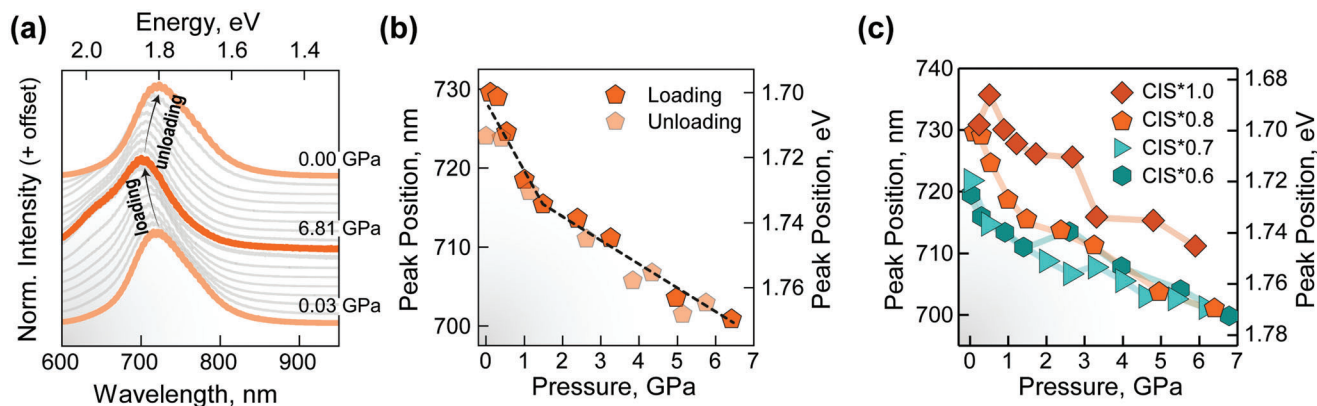


Figure 4. Calibration of the stoichiometry series. a) Emission spectra under 532-nm excitation during compression and decompression cycles in a DAC. b) Peak position in wavelength and energy versus applied pressure for the CIS*0.8 sample obtained from the compression and decompression cycles. The black dashed line is the double-linear fit to the experimental data. c) Comparison of the peak position change as a function of applied pressure during the compression cycle for all the samples of the stoichiometry series.

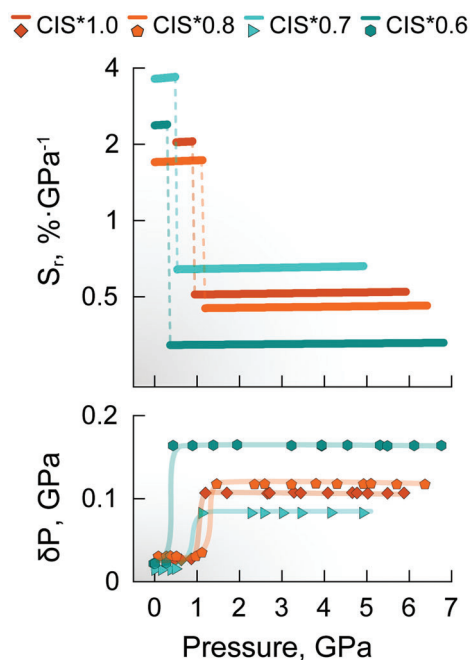


Figure 5. Comparison of the performance of the nanomanometers. Relative manometric sensitivity (top) and uncertainty (bottom) for the samples of the stoichiometry series.

which translates to two different regimes of S_r and δP (Figure 5). The parameters for the fitting of the curves used for the calculation of S_r and δP values reported in Figure 5 are displayed in Table S4 (Supporting Information). The applicability range of sample CIS*1.0 is limited to values > 0.5 GPa, due to the initial redshift. This is not the case for the samples with a lower amount of Cu^+ . Among them, CIS*0.7 shows the highest S_r value of $3.7\% \text{ GPa}^{-1}$ below 0.5 GPa, which decreases to $\approx 0.7\% \text{ GPa}^{-1}$ at higher pressures. These higher values of sensitivity also translate to lower uncertainties (0.02 and 0.09 GPa, respectively for the two ranges described above). A comparison of the performance of the presented QDs with other luminescent manometers re-

ported in the literature could be found in Table S5 (Supporting Information). Moreover, the cross-sensitivity of the QDs toward temperature and pressure was tested, recording the emission of the best-performing sample (CIS*0.7) as a function of temperature in the $20\text{--}50$ °C range (Figure S23, Supporting Information). Changes of $0.06 \text{ nm } ^\circ\text{C}^{-1}$ were observed, which correspond to uncertainty in the pressure readout of $<0.013 \text{ GPa } ^\circ\text{C}^{-1}$ throughout the whole tested range (see Table S6, Supporting Information for calculations).

Importantly, the discontinuity in the values of pressure sensitivity and uncertainty (Figure 5) does not preclude the use of these QDs as luminescent nanomanometers: It rather makes them more precise sensors for low values of pressure. Coincidentally, this aspect is beneficial when envisaging optimization of the QDs as nanomanometers for biological applications. If we consider an approximate edge length of 3.5 nm for the studied QDs, this translates to a tetrahedron surface area of 21.2 nm^2 . During the application of 1 GPa of pressure, the QD experiences therefore $\approx 20 \text{ nN}$ of mechanical force.

Hence the luminescent nanomanometers herein investigated can theoretically sense forces below 20 nN . This feature makes them attractive luminescent nanomanometers to study biological systems, such as focal adhesion forces of cells to their substrates and cell contractile forces exerted during, e.g., wound healing and regeneration studies.^[1,2b,28]

3. Conclusion

We have studied how size and composition play a role in the performance of CuInS_2 QDs as luminescence nanomanometers. Two series of samples were prepared changing their size – by tuning the reaction time – and composition – by varying the amount of copper introduced in the reaction mixture. Investigation in a diamond anvil cell revealed that CIS QDs with an intermediate size ($2.8\text{--}4.0 \text{ nm}$) afforded a lack of hysteresis, good sensitivity, and a larger operational working range. Control of the stoichiometry of CIS QDs of the selected size via the introduction of copper vacancies, then, allows to simultaneously increase the photoluminescence quantum yield (up to 7%) and the sensitivity (up to

3.5% GPa⁻¹ for pressures < 0.5 GPa) to externally applied mechanical pressure.

Overall, the results presented herein demonstrate that CIS QDs can perform as luminescent nanomanometers in pressure and force range of interest for biology, while keeping at minimum concerns over their toxicity, thanks to the lack of metals like cadmium and lead. In this sense, future efforts will be devoted to the transfer of CIS QDs to aqueous media and the investigation of their performance as luminescent nanomanometers in biological systems. In addition, the study of the behavior at the single-particle level of CuInS₂ QDs could provide insight into the effect that non-homogeneous size distribution and interparticle optical variability have on their overall performance as nanomanometers.

4. Experimental Section

Chemicals and Materials: Indium(III) acetate (In(OAc)₃, 99.99%), Copper(I) iodide (CuI, 98%), and Oleic Acid, 90% were purchased from Alfa Aesar. 1-Dodecanethiol (DDT, 98%), 1-Octadecene (ODE, 90%), and Ethyl Acetate (EtAc, 99%) were purchased from Thermo Scientific. Toluene (99.8%) and Acetone (99.6%) were purchased from Labkem. Methanol (MeOH, ≥99.9%) was purchased from Fisher scientific. Mineral oil was purchased from Sigma–Aldrich. All chemicals were used as received.

CuInS₂ QD Synthesis: In a typical synthesis of CuInS₂ QDs, 0.2 mmol (59.12 mg) of In(OAc)₃, 0.2 mmol (38.09 mg) of CuI, 4 mL of DDT and 10 mL of ODE were introduced in a 50-mL three-neck round-bottom flask. The mixture was put under vacuum and heated at 120 °C for 30 min. After this amount of time, the mixture turned clear yellow and was transferred to five 10-mL Pyrex vessel, which were flushed with Ar for a few seconds and later capped. Each vessel was subsequently introduced in a CEM Discover 2.0 MW reactor and rapidly heated to 240 °C. The reaction was allowed to proceed for a predetermined amount of time (between 2.5 to 10 min, in 2.5-min steps), during which the mixture gradually turned from yellow to dark red/brown. Subsequently, the dispersion was rapidly cooled to 70 °C with a stream of compressed air. The QDs were washed precipitating them with 4 mL of acetone, followed by centrifugation for 10 min at 3820 rcf. The supernatant was discarded and the QDs redispersed in 3 mL of toluene. This process was repeated two more times. The washed QDs were redispersed in 3 mL of toluene along with 30 μL each of OA and DDT to ensure colloidal stability over time. To control the stoichiometry of the CIS QDs, the 0.2 mmol of In(OAc)₃ were kept constant, while the CuI amount was reduced (0.16 mmol for 1:0.8, 0.14 mmol for 1:0.7, and 0.12 mmol for 1:0.6).

Transfer to Mineral Oil: Fifty μL of each QD dispersion was placed in a 1.5-mL centrifuge tube together with 300 μL of EtAc and 150 μL of MeOH. The dispersion was centrifuged at 9168 rcf and the supernatant was discarded. Fifty μL of mineral oil was added to the QDs and the dispersion was gently heated with the help of a hair drier to evaporate any residual solvent.

Physicochemical Characterization: Transmission electron microscopy (TEM) images were taken on two instruments: Jeol F200, Cold FEG and JEM 1010 JEOL with a CMOS TemCam F416 VIPs camera.

X-ray powder diffraction (XRPD) measurements were performed on a Rigaku D/max-γB diffractometer working in the Bragg-Brentano geometry (θ–2θ) with a step of 0.03° in the 20–60° range. The composition of copper indium sulfide QDs was determined via total reflection X-ray fluorescence (TXRF) with a S2 PICOFOX (Bruker).

Optical Characterization: The optical extinction spectra were recorded at room temperature on a UV–vis–NIR spectrophotometer (Perkin Elmer Lambda1050) using a 3-nm step in the 400–860 nm range. Photoluminescence spectra were recorded at room temperature on a home-made confocal fluorescence microscopy, using a 50-mW 488 nm solid-state laser as an excitation source and a high-sensitivity silicon CCD camera (Synapse,

Horiba) coupled to a monochromator (iH320, Horiba) as a detector. To investigate the evolution of the photoluminescence of CIS QDs with temperature, a Peltier temperature controller (Q-pod 2e, Quantum Northwest) was used. Measurements were taken every 5 °C using 10 min of thermal stabilization in the 20–50 °C range. For the detection, an OCEAN-HDX miniature spectrophotometer (Ocean Insight) was used.

Photoluminescence Measurements as a Function of Applied Pressure: Luminescence spectra at high pressure were acquired using a commercial scanning confocal Raman instrument (Renishaw InVia) exciting with a cw diode laser at 532 nm and detecting using a cooled CCD. A 20x SLWD objective was used to achieve a laser-spot diameter of <5 μm on the sample. High pressure was generated with a diamond anvil cell (mini-DAC) designed at the University of Paderborn (Germany). A 200 μm Inconel gasket was pre-indented to 70 μm to make the pressure chamber with a diameter of 150 μm. Ruby fluorescence was employed for calibration purposes and mineral oil was used as a pressure transmitting medium (PTM), providing quasi-hydrostatic pressures of up to 10.5 GPa.

Calculation of Relative Sensitivity and Uncertainty: The relative sensitivity (S_r) was calculated according to the following equation:

$$S_r = \frac{1}{\lambda} \left| \frac{\partial \lambda}{\partial P} \right| \quad (1)$$

The derivative was taken after fitting the experimental calibration curve to a linear function as described in the main text and shown in Figures S19 and S21 (Supporting Information).

To calculate the pressure uncertainty (i.e., resolution), 20 spectra were recorded at the same pressure (1 GPa, Figure S24, Supporting Information), and the position of the maximum extracted was described in Section S3.3 (Supporting Information). The standard deviation (σ) on the peak position at a fixed pressure was 0.38 nm.

For the calculation of the uncertainty, the following equation was used:

$$\delta P = \frac{\sigma}{\lambda_{\max}} \frac{1}{S_r} \quad (2)$$

where λ_{\max} is the position of the peak maximum.

Supporting Information

Supporting Information is available from the Wiley Online Library or from the author.

Acknowledgements

This work was supported by the Comunidad de Madrid (S2022/BMD-7403 RENIM-CM). A.B. acknowledges funding from Comunidad de Madrid through TALENTO grant ref. 2019-T1/IND-14014. R.M. is grateful to the Spanish Ministerio de Ciencia e Innovación for support to research through a Ramón y Cajal Fellowship (RYC2021-032913-I). U.R.R.M. & V.L. thank the Spanish Ministerio de Ciencia e Innovación for the project under the National Program of Sciences and Technological Materials (PID2019-106383GB-I1), and also the EU-FEDER funds.

Conflict of Interest

The authors declare no conflict of interest.

Data Availability Statement

The data that support the findings of this study are available from the corresponding author upon reasonable request.

Keywords

CuInS₂, luminescence, nanomanometry, pressure sensing, quantum dots

Received: May 9, 2023

Revised: July 31, 2023

Published online:

- [1] R. D. Mehlenbacher, R. Kolbl, A. Lay, J. A. Dionne, *Nat. Rev. Mater.* **2017**, 3, 17080.
- [2] a) A. Lay, D. S. Wang, M. D. Wisser, R. D. Mehlenbacher, Y. Lin, M. B. Goodman, W. L. Mao, J. A. Dionne, *Nano Lett.* **2017**, 17, 4172; b) W. Xu, R. Mezencev, B. Kim, L. Wang, J. McDonald, T. Sulchek, *PLoS One* **2012**, 7, e46609; c) Y. Zhang, C. Ge, C. Zhu, K. Salaita, *Nat. Commun.* **2014**, 5, 5167; d) L. Sikic, E. Schulman, A. Kosklin, A. Saraswathibhatla, O. Chaudhuri, J. Pokki, *Nano Lett.* **2022**, 22, 7742.
- [3] S. S. Hur, J. H. Jeong, M. J. Ban, J. H. Park, J. K. Yoon, Y. Hwang, *BMB Rep.* **2020**, 53, 74.
- [4] a) P. Roca-Cusachs, V. Conte, X. Trepast, *Nat. Cell Biol.* **2017**, 19, 742; b) O. Campàs, *Semin Cell Dev Biol* **2016**, 55, 119.
- [5] a) M. A. Antoniak, S. J. Zelewski, R. Oliva, A. Žak, R. Kudrawiec, M. Nyk, *ACS Appl. Nano Mater.* **2020**, 3, 4209; b) J. Wang, H. Ning, J. Wang, S. V. Kershaw, L. Jing, P. Xiao, *ACS Appl. Nano Mater.* **2022**, 5, 5617.
- [6] J. R. Casar, C. A. McLellan, C. Siefe, J. A. Dionne, *ACS Photonics* **2021**, 8, 3.
- [7] a) M. Runowski, J. Marciniak, T. Grzyb, D. Przybylska, A. Shyichuk, B. Barszcz, A. Katrusiak, S. Lis, *Nanoscale* **2017**, 9, 16030; b) M. Runowski, P. Woźny, I. R. Martín, *J. Mater. Chem. C* **2021**, 9, 4643.
- [8] M. Szymczak, M. Runowski, M. G. Brik, L. Marciniak, *Chem. Eng. J.* **2023**, 466, 143130.
- [9] K. K. Zhuravlev, J. M. Pietryga, R. K. Sander, R. D. Schaller, *Appl. Phys. Lett.* **2007**, 90, 043110.
- [10] a) Y.-C. Lin, W.-C. Chou, A. S. Susa, S. V. Kershaw, A. L. Rogach, *Nanoscale* **2013**, 5, 3400; b) C. T. Yuan, Y. C. Lin, Y. N. Chen, Q. L. Chiu, W. C. Chou, D. S. Chuu, W. H. Chang, H. S. Lin, R. C. Ruaan, C. M. Lin, *Nanotechnology* **2007**, 18, 185402; c) H. Zhong, Y. Zhou, M. Ye, Y. He, J. Ye, C. He, C. Yang, Y. Li, *Chem. Mater.* **2008**, 20, 6434.
- [11] a) B. Zhou, G. Xiao, X. Yang, Q. Li, K. Wang, Y. Wang, *Nanoscale* **2015**, 7, 8835; b) G. M. Biesold, S. Liang, B. Brettmann, N. Thadhani, Z. Kang, Z. Lin, *Angew. Chem. Int. Ed.* **2021**, 60, 9772.
- [12] a) G. Morselli, M. Villa, A. Fermi, K. Critchley, P. Ceroni, *Nanoscale Horiz.* **2021**, 6, 676; b) J. Kolny-Olesiak, H. Weller, *ACS Appl. Mater. Interfaces* **2013**, 5, 12221.
- [13] J. C. Kays, A. M. Saeboe, R. Toufanian, D. E. Kurant, A. M. Dennis, *Nano Lett.* **2020**, 20, 1980.
- [14] R. Marin, A. Vivian, A. Skripka, A. Migliori, V. Morandi, F. Enrichi, F. Vetrone, P. Ceroni, C. Aprile, P. Canton, *ACS Appl. Nano Mater.* **2019**, 2, 2426.
- [15] S. I. Pokutnyĭ, *Semiconductors* **2007**, 41, 1323.
- [16] M. Booth, A. P. Brown, S. D. Evans, K. Critchley, *Chem. Mater* **2012**, 24, 2064.
- [17] a) J. Tauc, R. Grigorovici, A. Vancu, *Phys. Status Solidi B* **1966**, 15, 627; b) P. Makuła, M. Pacia, W. Macyk, *J. Phys. Chem. Lett.* **2018**, 9, 6814.
- [18] a) B. Chen, H. Zhong, W. Zhang, Z. a. Tan, Y. Li, C. Yu, T. Zhai, Y. Bando, S. Yang, B. Zou, *Adv. Funct. Mater.* **2012**, 22, 2081; b) K. E. Knowles, H. D. Nelson, T. B. Kilburn, D. R. Gamelin, *J. Am. Chem. Soc.* **2015**, 137, 13138.
- [19] X.-F. Zhang, Y. Zhang, L. Liu, *J. Lumin.* **2014**, 145, 448.
- [20] T. P. van Swieten, A. Meijerink, F. T. Rabouw, *ACS Photonics* **2022**, 9, 1366.
- [21] a) E. Pedrueza, A. Segura, R. Abargues, J. B. Bailach, J. C. Chervin, J. P. Martínez-Pastor, *Nanotechnology* **2013**, 24, 205701; b) J. C. Beimbom, II, L. R. Walther, K. D. Wilson, J. M. Weber, *J. Phys. Chem. Lett.* **2020**, 11, 1975.
- [22] S. FANA, Z. LUB, *Thermal Science* **2022**, 26, 2823.
- [23] a) E. Mazalan, M. Aziz, N. Amin, F. Ismail, M. Roslan, K. Chaudhary, *J. Phys.: Conf. Ser.* **2023**, 2432, 012009; b) J.-W. Yang, L. An, *Solid State Commun.* **2020**, 316–317, 113952.
- [24] Y. Li, Y. Wang, R. Tang, X. Wang, P. Zhu, X. Zhao, C. Gao, *J. Phys. Chem. C* **2015**, 119, 2963.
- [25] a) K. Bian, B. T. Richards, H. Yang, W. Bassett, F. W. Wise, Z. Wang, T. Hanrath, *Phys. Chem. Chem. Phys.* **2014**, 16, 8515; b) R. Cherian, C. Gerard, P. Mahadevan, N. T. Cuong, R. Maezono, *Phys. Rev. B* **2010**, 82, 235321.
- [26] Z. Chen, J. C. Beimbom, II, N. Kirkwood, S. P. Russo, J. M. Weber, P. Mulvaney, *J. Phys. Chem. C* **2023**, 127, 8657.
- [27] A. Lay, C. Siefe, S. Fischer, R. D. Mehlenbacher, F. Ke, W. L. Mao, A. P. Alivisatos, M. B. Goodman, J. A. Dionne, *Nano Lett.* **2018**, 18, 4454.
- [28] B. A. Harley, T. M. Freyman, M. Q. Wong, L. J. Gibson, *Biophys. J.* **2007**, 93, 2911.